







RESEARCH ARTICLE | APRIL 10 2024

Reliable operation of Cr₂O₃:Mg/β-Ga₂O₃ p–n heterojunction diodes at 600 °C ^{EP}

Special Collection: (Ultra)Wide-bandgap Semiconductors for Extreme Environment Electronics

William A. Callahan ; Kingsley Egbo ; Cheng-Wei Lee ; David Ginley ; Ryan O'Hayre ; Andriy Zakutayev 

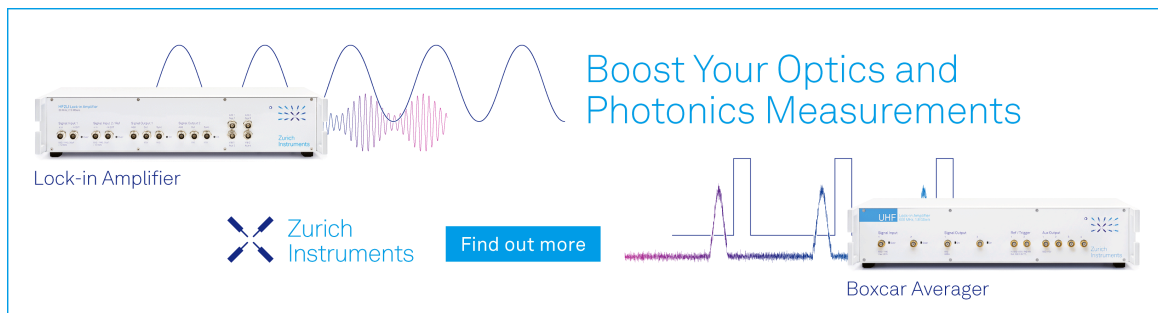
 Check for updates

Appl. Phys. Lett. 124, 153504 (2024)
<https://doi.org/10.1063/5.0185566>




26 April 2024 19:54:56

Boost Your Optics and Photonics Measurements



Lock-in Amplifier

 Zurich Instruments

[Find out more](#)

Boxcar Averager

Reliable operation of Cr₂O₃:Mg/ β -Ga₂O₃ p-n heterojunction diodes at 600 °C

Cite as: Appl. Phys. Lett. **124**, 153504 (2024); doi: [10.1063/5.0185566](https://doi.org/10.1063/5.0185566)

Submitted: 31 October 2023 · Accepted: 21 March 2024 ·

Published Online: 10 April 2024






View Online



Export Citation



CrossMark

William A. Callahan,^{1,2,a)}  Kingsley Egbo,¹  Cheng-Wei Lee,³  David Ginley,¹  Ryan O'Hayre,³ 
and Andriy Zakutayev^{1,a)} 

AFFILIATIONS

¹Materials Science Center, National Renewable Energy Laboratory, Golden, Colorado 80401, USA

²Advanced Energy Systems Graduate Program, Colorado School of Mines, Golden, Colorado 80401, USA

³Department of Metallurgical and Materials Engineering, Colorado School of Mines, Golden, Colorado 80401, USA

Note: This paper is part of the APL Special Collection on (Ultra)Wide-bandgap Semiconductors for Extreme Environment Electronics.

^{a)}Authors to whom correspondence should be addressed: will.callahan@nrel.gov and andriy.zakutayev@nrel.gov

ABSTRACT

Beta gallium oxide (β -Ga₂O₃)-based semiconductor heterojunctions have recently demonstrated improved performance at high voltages and elevated temperatures and are, thus, promising for applications in power electronic devices and harsh environment sensors. However, the long-term reliability of these ultra-wideband gap (UWBG) semiconductor devices remains barely addressed and may be strongly influenced by chemical reactions at the p-n heterojunction interface. Here, we experimentally demonstrate operation and evaluate the reliability of Cr₂O₃:Mg/ β -Ga₂O₃ p-n heterojunction diodes during extended operation at 600 °C, as well as after 30 repeated cycles between 25 and 550 °C. The calculated pO₂-temperature phase stability diagram of the Ga-Cr-O material system predicts that Ga₂O₃ and Cr₂O₃ should remain thermodynamically stable in contact with each other over a wide range of oxygen pressures and operating temperatures. The fabricated Cr₂O₃:Mg/ β -Ga₂O₃ p-n heterojunction diodes show room-temperature on/off ratios >10⁴ at \pm 5 V and a breakdown voltage (V_{Br}) of -390 V. The leakage current increases with increasing temperature up to 600 °C, which is attributed to Poole-Frenkel emission with a trap barrier height of 0.19 eV. Over the course of a 140-h thermal soak at 600 °C, both the device turn-on voltage and on-state resistance increase from 1.08 V and 5.34 m Ω cm² to 1.59 V and 7.1 m Ω cm², respectively. This increase is attributed to the accumulation of Mg and MgO at the Cr₂O₃/Ga₂O₃ interface as observed from the time-of-flight secondary ion mass spectrometry analysis. These findings inform future design strategies of UWBG semiconductor devices for harsh environment operation and underscore the need for further reliability assessments for β -Ga₂O₃-based devices.

© 2024 Author(s). All article content, except where otherwise noted, is licensed under a Creative Commons Attribution (CC BY) license (<https://creativecommons.org/licenses/by/4.0/>). <https://doi.org/10.1063/5.0185566>

Beta gallium oxide (β -Ga₂O₃) is a prime candidate for next-generation sensing and power electronic devices, especially for high-temperature applications. Due to its large bandgap and high theoretical breakdown field, β -Ga₂O₃ shows promise for high-voltage operation and high-frequency switching. Additionally, β -Ga₂O₃ can be doped *n*-type to relatively high levels, most commonly with Si and Sn. Single-crystal β -Ga₂O₃ can be grown via multiple bulk methods, including Czochralski (CZ) and edge-defined film-fed growth (EFG). Techno-economic analysis and projective cost modeling suggests that further development of Ga₂O₃-based technologies will improve their commercial viability in competition with current SiC and GaN technologies.¹⁻⁶

Over the last few years, significant progress has been made in expanding the capabilities of β -Ga₂O₃ devices toward high-performance operation, with several groups making efforts to reach the predicted theoretical high-power limits via maximization of breakdown voltage and simultaneous minimization of on-state resistance. This has been achieved through a shift from relatively simple Schottky/heterojunction device structures toward more complex stacks that incorporate field plates, guard rings, and dielectric layers.⁷ However, there are a few operational demonstrations of these devices at high temperature, specifically above 300–400 °C, and even fewer that study performance stability.⁸ Previously, we found that a combination of repeated cycling between low and high temperatures

(“cycling”), as well as long-term exposure to very high temperatures (“soaking”), provides insight into both mechanical and thermodynamic stressors that can degrade device electrical performance.^{9,10}

A variety of *p*-type materials have been explored for use in β -Ga₂O₃ device fabrication, including SiC, GaN, NiO, diamond, SnO, and Cu₂O.^{11–16} Nickel oxide (NiO) is the most widely explored due to its wide bandgap and favorable band alignment with β -Ga₂O₃, achieving turn-on voltages in the range of 0.9–1.8V and reliably low leakage currents during room-temperature operation. Furthermore, very high breakdown voltages and excellent corresponding Baliga figures of merit have been reported for NiO/ β -Ga₂O₃ heterojunctions.^{17–27} Of the candidate *p*-type metal oxides for use in β -Ga₂O₃ device fabrication, several (e.g., Cu₂O and NiO) are predicted to form ternary compounds when in contact with Ga₂O₃ based on computational thermodynamics.²⁸ Here, we report β -Ga₂O₃ heterojunction diodes using the wide bandgap *p*-type chromium oxide (Cr₂O₃), for which there is virtually no literature. However, recent XPS work on Ga₂O₃/Cr₂O₃ suggests favorable band alignment ($\Delta E_C = 1.68$ eV and $\Delta E_V = 3.38$ eV) for heterojunction device fabrication.^{29,30}

In this work, epitaxial Cr₂O₃:Mg/ β -Ga₂O₃ vertical pn-diodes are fabricated, and their electrical performance and thermal reliability are evaluated. The diodes show a room-temperature rectification ratio $>10^4$ at ± 5 V and a breakdown voltage of -390 V. We then subject several Cr₂O₃:Mg/ β -Ga₂O₃ heterojunction diodes to repeated thermal cycling between 25 and 550 °C, as well as separately to a 140-h thermal soak at 600 °C. We find that the devices show exceptionally stable reverse bias leakage current during prolonged high-temperature testing, but experience forward-bias changes in the form of increased on-state resistance, turn-on voltage, and forward current drop. The reverse bias leakage current can be described by Poole–Frenkel emission (PFE) with a trap barrier height of 0.19 eV. We attribute the observed evolution in the forward bias electrical properties to the accumulation

of Mg and MgO at the Cr₂O₃/Ga₂O₃ interface after prolonged operation at 600 °C due to the temperature induced diffusion of the Mg dopants in Cr₂O₃. This study provides insights and design considerations for oxide-based ultra-wideband gap (UWBG) semiconductors for p–n heterojunctions applicable in harsh operating environments.

Figure 1(a) shows the calculated oxygen partial pressure vs temperature (pO_2 - T) phase diagrams for the Ga–Cr–O system. The “Experimental Range” box includes the temperature and pO_2 conditions used in this report, which are limited by instrumentation. Cr₂O₃ and Ga₂O₃ are predicted to coexist for effectively all desirable temperatures and oxygen partial pressures. This pO_2 - T phase diagram for the Ga–Cr–O system was calculated using density functional theory (DFT) datasets from NREL MatDB^{31,32} along with correction schemes^{33,34} to achieve chemical accuracy (~ 50 meV/atom). Specifically, we estimate the Gibbs formation energy of a compound, $\Delta G_f(T)$, in units of eV/atom by

$$\Delta G_f(T) = \Delta H_f(298.15K) + G_{SISSO}^\delta(T) - \sum_i \alpha_i G_{i,exp}(T), \quad (1)$$

where $\Delta H_f(298.15K)$ is the standard formation enthalpy of the compound and is calculated using DFT total energies from the NREL MatDB and fitted elemental-phase reference energies. Here, α_i is the stoichiometric weight for element *i* in the compound using experimental values from FactSage³⁵ for absolute Gibbs free energy of element *i*. $G_{SISSO}^\delta(T)$ (eV/atom) captures temperature dependency of the compound due to phonons.³⁴ Finally, we collect $\Delta G_f(T)$ for all competing phases and use convex hull analysis to calculate the grand potential phase diagram. The ideal gas law, e.g., $\Delta\mu_O = \frac{1}{2}k_B T \ln(pO_2)$, is used to connect oxygen chemical potential (μ_O) to oxygen partial pressure (pO_2) in units of atm, where $\Delta\mu_O$ is the deviation from the standard oxygen chemical potential (μ_O°) with $\mu_O = \mu_O^\circ + \Delta\mu_O$.³⁶ A full description of these calculations is available online.³⁷

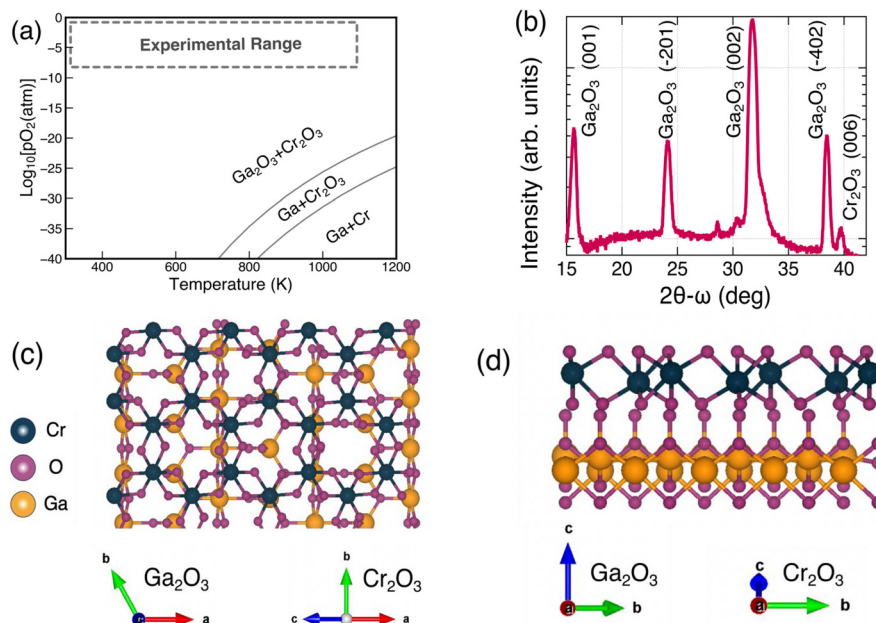


FIG. 1. (a) Calculation showing pO_2 -temperature phase stability diagram for the Ga–Cr–O system. The “Experimental Range” box highlights the expected operating conditions for devices made from these materials, including the conditions used in this report. (b) 2θ - ω scan of a 120 nm Cr₂O₃:Mg layer grown on (001) HVPE Ga₂O₃ substrate on a log scale. The region 36° – 42° shows both the (-201) sublattice of the HVPE layer and the preferential growth of (006) Cr₂O₃ on that sublattice. (c) Top-down and (d) profile views of the (001) Cr₂O₃–(001) Ga₂O₃ interface.

Cr₂O₃:Mg was deposited via pulsed laser deposition (PLD). During PLD growth, a ceramic target of 8 at. % Mg-doped Cr₂O₃ was ablated using a pulsed KrF excimer laser at a frequency of 10 Hz and energy of 300 mJ. Growth was performed at a substrate temperature of 600 °C and O₂ partial pressure of 3×10^{-4} Torr. To fabricate Ohmic contacts (Fig. S1), Cr₂O₃:Mg was grown on a c-sapphire substrate, followed by a bi-metal deposition of 5 nm Ti/100 nm Au. E-beam evaporation of metals was performed with a Temescal FC2000 evaporation system under high vacuum conditions ($\leq 3 \times 10^{-6}$ Torr) without venting between layers. Room-temperature Hall measurements were performed with a Lakeshore FastHall system. The Cr₂O₃:Mg films were determined to be *p*-type with a carrier concentration of 2.4×10^{17} cm⁻³; a resistivity of 31.5 Ω cm, which is in good agreement with reports on Mg-doped Cr₂O₃,^{38,39} and a mobility of 0.82 cm² V⁻¹ s⁻¹, which can be significantly improved with choice of dopant.⁴⁰ High-temperature Hall measurements were also attempted using a custom instrument,⁴¹ but the results were inconclusive. To electrically test the Ohmic contacts to Cr₂O₃:Mg, two-probe measurements (source I, measure V) were performed via a Keithley 236 SMU in a custom McAllister probe station in ambient air. IV curves were collected every 15 min. To initiate the long-term thermal soak, the probe station was ramped to 600 °C at a rate of 100 °C per hour. Over the course of the one week testing period at 600 °C, the resistance remains effectively constant, and the IV curves remain linear. Electrical measurements reveal that Cr₂O₃:Mg is a highly resistive semiconductor, especially at lower temperatures. Full results and figures for the Ohmic contact testing can be found in the supplementary material, Fig. S1.

Figure 1(b) gives a 2θ - ω scan of a 120 nm Cr₂O₃:Mg layer grown on (001) Si-doped HVPE Ga₂O₃ substrate, performed using a Bruker 8 Discover diffractometer. In addition to the (001) Ga₂O₃ planes, there are also peaks that indicate the presence of a (-201) Ga₂O₃ sublattice within the HVPE layer. In the region from 36° to 42°, the (006) plane of Cr₂O₃ can be observed and its proximity to the (-402) plane of Ga₂O₃ suggests preferential growth on this sublattice. This relationship is further supported by Fig. S4, which shows a similar 2θ - ω scan of Cr₂O₃:Mg layer preferentially growing in the (001) orientation on a reference (-201) β-Ga₂O₃ substrate. Figures 1(c) and 1(d) give a top-down and profile visualization of the stacked (001) planes for both materials in the Cr₂O₃-Ga₂O₃ relationship, respectively.

Cr₂O₃:Mg/β-Ga₂O₃ p-n vertical heterojunction devices were fabricated using 1 μm thick β-Ga₂O₃ drift layers ($n \cong 4 \times 10^{16}$ cm⁻³) grown via HVPE on (001) Ga₂O₃:Sn from Novel Crystal Technologies.

Photoresist was removed from the as-delivered substrates via an organic wash, followed by a sulfuric acid/peroxide rinse. Next, large-area back Ohmic contacts (5 nm Ti/100 nm Au) and the *p*-Cr₂O₃:Mg layer were deposited via e-beam and PLD, respectively, via the methods previously described. Two different geometries were used for the top Ohmic contacts to Cr₂O₃:Mg. For the thermal cycling devices, shadow masks were used to define an array of 1 mm diameter pads that were sufficiently large to ensure reliable probe contact despite repeated thermal expansion and contraction. To fabricate devices for the long-term thermal soak, contact aligner lithography was used to make circular pads of increasing size, from 50 to 300 μm in diameter. In both cases, the 5 nm Ti/100 nm Au contacts were deposited as before. Following contact deposition, both Ohmic and heterojunction samples were annealed a single time via rapid thermal processing (ULVAC-RIKO MILA-3000 Rapid Thermal Processing Unit) at 550 °C for 90 s in flowing N₂.

Figure 2 gives the room-temperature electrical characteristics of a 300 μm diameter Cr₂O₃:Mg/β-Ga₂O₃ p-n diode under 50 sccm flowing Ar. Figure 2(a) shows the entire JV characteristic on a log scale, measured from +5 to -10 V. A rectification ratio greater than 10⁴ is achieved at ±5 V. The diode reaches a turn-on current density of 1 A/cm² at approximately 1.65 V, and fitting of the “On” portion of the curve on a linear scale (Fig. S2) yields an R_{on} of 12.96 mΩ cm². The inset shows the device p-n heterojunction architecture for devices studied in this report. The details about doping levels and layer thicknesses can be found in Fig. S2. Figure 2(b) gives a reverse bias breakdown voltage of 0.39 kV. Room-temperature breakdown voltage was measured using a Keysight B1505A Power Device Analyzer with a reverse current limit of 1 mA. Significant further improvements can be expected based on architectural enhancements to control the electric field and optimize the growth conditions.

Both thermal cycling and soaking of the heterojunction diodes were performed with a Keithley 2635 A SMU in an Instec HCP621G-PMH temperature-controlled probe station. Thermal cycling consists of repeated ramping from 25 to 550 °C and back down in steps of 75 °C. The instrument was allowed to equilibrate for 15–20 min at each temperature before electrical measurements were collected. Thermal soaking was performed in a similar fashion; the instrument was manually ramped from 25 to 600 °C in steps of 75–100 °C. The instrument was allowed to equilibrate for 20–30 min at each temperature, after which electrical measurements were collected. Upon reaching 600 °C, electrical measurements were performed every 30 min for the full duration of the soaking experiment. For thermal cycling, IV

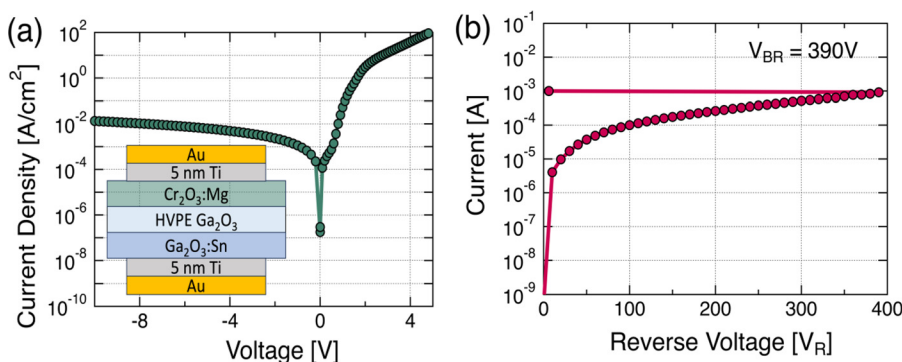


FIG. 2. (a) Room-temperature JV characteristics for 300 μm Cr₂O₃:Mg/β-Ga₂O₃ p-n heterojunction diode, shown in forward bias on a linear scale. Inset shows the device architecture of the p-n heterojunctions used in this report. (b) Room-temperature reverse bias breakdown performance.

curves were collected from $0 \rightarrow +5$ V, followed by a reverse bias sweep from $0 \rightarrow -20$ V. Compliance was set to 0.1 A for all measurements. For thermal soaking electrical measurements, IV curves were collected from $0 \rightarrow +5$ V with a 0.2 A current limit, followed by a reverse bias sweep from $0 \rightarrow -10$ V with a 0.1 A current limit.

Figure 3 shows the high-temperature reliability of several Cr_2O_3 :Mg/ β - Ga_2O_3 pn diodes under both thermal soaking and cycling conditions. Figure 3(a) shows results of a >100 -h thermal soak at 600°C for a $300\ \mu\text{m}$ Cr_2O_3 :Mg/ β - Ga_2O_3 pn diode under 50 sccm flowing Ar. JV curves were measured every 30 min, with traces plotted every 10 h to demonstrate the time evolution. A line was fit to the “On” portion of Fig. 3(a) from 100 to $250\ \text{A}/\text{cm}^2$ and extrapolated to determine the turn-on voltage and specific on-state resistance. After a break-in period of 10 h, V_{on} steadily increases from 1.08 to 1.59 V after 140 h, at a rate of approximately 4 mV per hour. Correspondingly, the value of R_{on} also increases from 5.34 to $7.1\ \text{m}\ \Omega\ \text{cm}^2$ over the same period but appears to grow with the square root of time. The evolution of reverse bias leakage currents was also examined and found to stabilize at all voltages after a break-in period of ~ 30 h. Plots of R_{on} , V_{on} , and J_{Rev} vs time can be found in Figs. S2(c)–S2(e). Figure S2(f) shows the forward-bias JV curves for the same $300\ \mu\text{m}$ Cr_2O_3 :Mg/ β - Ga_2O_3 pad taken before (“Pre,” solid lines) and after (“Post,” dashed lines) the 140-h soak at 600°C , measured out to $+5$ V. Significant changes in performance can be observed, especially at lower temperatures. Room-temperature V_{on} and R_{on} increase from 1.65 V and $12.96\ \text{m}\ \Omega\ \text{cm}^2$ to 3.84 V and $312\ \text{m}\ \Omega\ \text{cm}^2$, respectively.

To understand the cause of the increase in forward drop, both the thermally soaked (“test”) sample and an as-deposited (“reference”) sample were studied using time-of-flight secondary ion mass spectrometry (TOF-SIMS) analysis. The results are shown in Fig. 3(b) and Fig. S5. The test sample reveals a significant amount of Mg dopant diffusing to the Cr_2O_3 / Ga_2O_3 interface after thermal soaking at 600°C .

Beyond this, there appears to be no interdiffusion of any other species between the p -type and n -type layers—the interface remains abrupt, which supports our theoretical calculations. The normalized Mg and MgO signals at the interface from the test and reference sample are also compared. Both signals at the Cr_2O_3 / Ga_2O_3 interface in the test sample are significantly higher than in the reference sample. While there is evidence of a small amount of Mg accumulation in the reference sample, very little of it appears to have oxidized. This diffusion can be attributed to the short-term high-temperature growth conditions experienced during PLD. MgO is a well-known wide bandgap material that is frequently used for its dielectric strength.⁴⁶ Given the band alignment of Ga_2O_3 with MgO and Cr_2O_3 ,^{29,47} this observed reaction amounts to inserting a thin dielectric layer between the p -type and n -type layers. Assuming the thickness of this MgO layer is increasing with time at temperature, this potentially explains the gradual increase in both forward bias resistance and turn-on voltage observed in the electrical measurements. The reverse bias leakage current stabilizes after 20–40 h, which suggests that the mechanism for current transport has a relatively low energy barrier and is not strongly dependent on the thickness of the Mg/MgO layer. While the final recorded turn-on voltage at 600°C approaches the band offset of Cr_2O_3 and Ga_2O_3 measured with XPS,^{29,30} it is more likely that this is attributable to the MgO layer. Temperature-dependent XPS measurements are needed to better understand this relationship.

A separate device utilizing 1 mm diameter pads was subject to repeated thermal cycling between 25 and 550°C , with current compliance set to 100 mA. Forward bias curves were measured out to 5 V; reverse bias was measured to -20 V. Figure 3(c) shows the forward-bias J-V-T curves for cycle 5 and cycle 30 for three different temperatures, showing slight increases in V_{on} with negligible changes in R_{on} . Figure 3(d) shows the evolution of leakage current with increasing

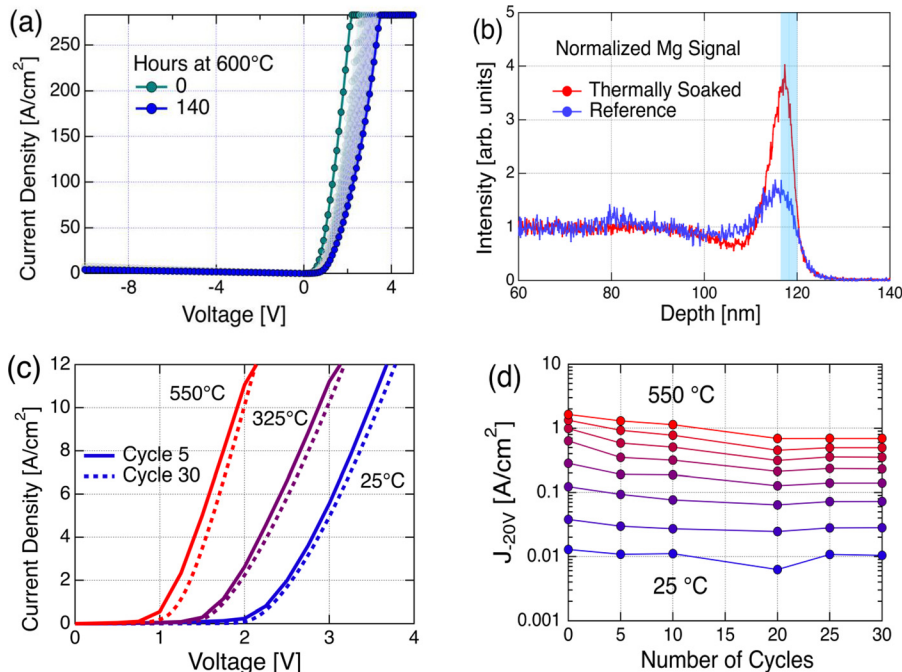


FIG. 3. (a) Linear JV curves of a $300\ \mu\text{m}$ diameter Cr_2O_3 :Mg/ β - Ga_2O_3 p-n diode operating at 600°C for 140 h, with traces plotted every 10 h. The current limits were set to 200 mA in forward bias and 100 mA in reverse bias to prevent damage during operation. (b) Normalized Mg signal from TOF-SIMS for the thermally soaked diode and an as-deposited reference device. The Ga_2O_3 / Cr_2O_3 interface is indicated by the blue rectangle. The signals have been normalized relative to their baseline signal taken from between 20 and 80 nm in the Cr_2O_3 layers. (c) Forward bias JV curves of a 1 mm diameter Cr_2O_3 :Mg/ β - Ga_2O_3 pn diode for three select soaked temperatures before and after repeated thermal cycling. (d) Evolution of temperature dependent leakage current with repeated cycling, measured at -20 V.

cycle, as measured at -20 V. With a few exceptions at lower temperature, the leakage current appears to stabilize after ~ 20 cycles.

Overall, Fig. 3 demonstrates the different effects of thermal cycling and thermal soaking on the performance of electronic devices. While both impart a significant thermal load, the 140-h soak at 600°C appears to have greater impact on device recovery, especially at lower temperatures. In contrast, the changes in electrical behavior between cycles 5 and 30 in the temperature cycling test are significantly less severe. In both experiments, the reverse bias leakage current stabilizes after a somewhat significant break-in period (~ 30 h or 20 cycles, respectively); the forward bias current appears to be more affected in both cases. Another consideration is the size of the pad being measured. Given the poor thermal conductivity of $\beta\text{-Ga}_2\text{O}_3$, it is possible that device performance degradation can be attributed to substantial Joule heating. Since there is a greater than ten-fold increase in the area of the thermally cycled devices when compared to those that were soaked, the generated heat can be more evenly distributed across the contact area.

To understand the corresponding leakage current mechanism, we examined reverse bias J-V-T measurements from cycle 30 [Fig. 4(a)]. The results show that reverse bias current has a strong dependence on both temperature and voltage. To analyze these results, we use the Poole-Frenkel emission (PFE) model, which describes conduction via thermal excitation of electrons from trap states and is typically present in insulating layers. PFE can be expressed by the following equation:

$$J_0 \propto E \exp\left(-\frac{q(\phi_F - \sqrt{qE/\pi\epsilon_s\epsilon_0})}{k_B T}\right). \quad (2)$$

Here, E is the electric field across the depletion region, ϕ_F is the barrier height of the trap state, ϵ_s is the relative dielectric constant, and k_B is Boltzmann's constant. To extract the barrier height of these trap states, graphs of $\ln\left(\frac{J}{E}\right)$ vs \sqrt{E} are first plotted for each temperature, showing excellent linear fits [Fig. 4(b)]. Subsequently, the intercepts of these linear fits are plotted against $q/k_B T$ (Fig. S3), yielding trap barrier heights of 0.191 eV.^{42–44} This relatively low barrier height is smaller than what has been reported for NiO/Ga₂O₃,⁴⁵ which results in the leakage current of the Cr₂O₃:Mg/ $\beta\text{-Ga}_2\text{O}_3$ diodes that is several orders of magnitude higher than NiO/Ga₂O₃ heterojunctions.

The J-V-T results and analysis presented in Fig. 4 indicate that the cycling and soaking reliability trends presented in Fig. 3 may be related to non-ideal interfaces in the overall Au/Ti/Cr₂O₃:Mg/

$\beta\text{-Ga}_2\text{O}_3$ /Ti/Au multi-layer device stack [Fig. 1(a), inset]. The contribution of Au/Ti/Cr₂O₃:Mg or $\beta\text{-Ga}_2\text{O}_3$ /Ti/Au Ohmic contacts to this device degradation can be ruled out. This is because the independent Au/Ti/Cr₂O₃:Mg/Al₂O₃ Ohmic contacts stability study (see Fig. S1) showed that they remain stable for a longer time than the device as a whole. Our earlier published results on $\beta\text{-Ga}_2\text{O}_3$ showed stable Ohmic behavior after >500 h of continuous operation at 600°C .⁹ Another potential interface where degradation can occur is Cr₂O₃:Mg/ $\beta\text{-Ga}_2\text{O}_3$. As shown in Fig. 1(b), there is a quasi-ordered relationship between the Cr₂O₃ layer and the (-201) character of the (001)-oriented HVPE Ga₂O₃ substrate. The lack of direct epitaxy can result in a lower interface quality, which can lead to a high density of interfacial trap states and thereby facilitate reverse bias conduction. Furthermore, this might be exacerbated by the accumulation of Mg and MgO at this interface. However, this is unlikely because similar lack of ideal epitaxy exists at the NiO/ $\beta\text{-Ga}_2\text{O}_3$ interface, which shows higher barrier extracted from the J-V-T measurement using the PFE model.⁴⁵ It is worth noting that based on the minimal changes to forward bias conduction and the shorter cumulative exposure time to high temperatures, we do not anticipate as much Mg/MgO migration in the thermally cycled samples as in the thermally soaked samples.

In this work, we demonstrate reliable operation of Cr₂O₃:Mg/ $\beta\text{-Ga}_2\text{O}_3$ p-n heterojunction diodes at 600°C . This experimental work is motivated by theoretical calculations that predict thermodynamically stable phase coexistence of $n\text{-Ga}_2\text{O}_3$ and $p\text{-Cr}_2\text{O}_3$ for an extremely wide range of temperatures and pO₂. We fabricate Cr₂O₃:Mg/ $\beta\text{-Ga}_2\text{O}_3$ vertical p-n heterojunction diodes with V_{on} , R_{on} , and V_{br} of 1.65 V, 12.96 m Ωcm^2 , and -390 V, respectively, at room temperature. We subject several diodes to repeated thermal cycling between 25 and 550°C and long-term continuous operation at 600°C for 140 h. The analysis of the reverse bias current shows that the leakage mechanism is very well described by Poole-Frenkel emission. We find that prolonged thermal soaking has more deleterious effects on electrical performance than repeated cycling, leading to increased turn-on voltage and on-state resistance. Since we observed stability of the ultrathin Ti/Au Ohmic contact to Cr₂O₃:Mg/c-Al₂O₃ as well as Ga₂O₃/Ti/Au contacts under the same high-temperature operating conditions, we attribute this performance evolution to the migration of Mg to the Cr₂O₃/Ga₂O₃ interface, where TOF-SIMS reveals the presence of a thin MgO layer. Future work should focus on understanding these degradation phenomena and their temperature dependence, as well as comparisons to other material systems under similar conditions.

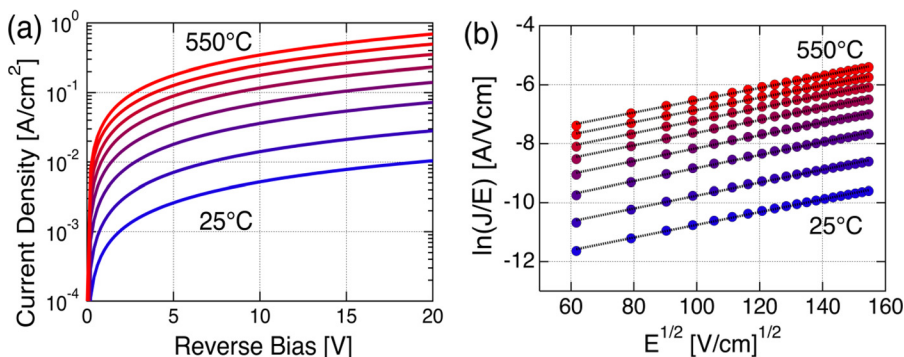


FIG. 4. (a) Reverse bias JV curves from cycle 30, showing dependence on both temperature and voltage. (b) Poole-Frenkel plots of leakage current for cycle 30, with linear fits to each temperature trace shown in dotted black lines.

See the supplementary material for (S1) device architecture for Ohmic contact devices; temperature-dependent performance of Ohmic contact; (S2) room-temperature and high-temperature JV curves of $\text{Cr}_2\text{O}_3:\text{Mg}/\beta\text{-Ga}_2\text{O}_3$ p-n devices, as well as extracted parameters from a 140-h soak at 600°C ; (S3) Poole-Frenkel barrier height extraction; (S4) XRD of (001) $\text{Cr}_2\text{O}_3:\text{Mg}/(-201)$ $\beta\text{-Ga}_2\text{O}_3$; and (S5) TOF-SIMS results for thermally soaked and reference $\text{Cr}_2\text{O}_3:\text{Mg}/\beta\text{-Ga}_2\text{O}_3$ samples.

This work was authored by the National Renewable Energy Laboratory (NREL), operated by Alliance for Sustainable Energy, LLC, for the U.S. Department of Energy (DOE) under Contract No. DE-AC36-08GO28308. Funding is provided by the Office of Energy Efficiency and Renewable Energy (EERE) Advanced Materials & Manufacturing Technologies Office. High-voltage breakdown measurements are supported by a laboratory directed research and development (LDRD) program at NREL. The views expressed in the article do not necessarily represent the views of the DOE or the U.S. Government. This material makes use of the TOF-SIMS system at the Colorado School of Mines, which was supported by the National Science Foundation under Grant No.1726898. We would especially like to thank V.S. for his contributions to the computational methods used in this report; C.E.P. for her assistance in high-temperature transport measurements; and M.A.W. for his analysis with the TOF-SIMS system.

AUTHOR DECLARATIONS

Conflict of Interest

The authors have no conflicts to disclose.

Author Contributions

William A. Callahan: Conceptualization (equal); Data curation (equal); Formal analysis (equal); Methodology (equal); Software (equal); Validation (equal); Visualization (equal); Writing – original draft (equal); Writing – review & editing (equal). **Kingsley Egbo:** Conceptualization (equal); Resources (lead); Writing – review & editing (equal). **Cheng-Wei Lee:** Software (equal); Visualization (supporting); Writing – review & editing (equal). **David Ginley:** Funding acquisition (equal); Supervision (equal); Writing – review & editing (equal). **Ryan O’Hayre:** Funding acquisition (equal); Supervision (equal); Writing – review & editing (equal). **Andriy Zakutayev:** Funding acquisition (equal); Project administration (equal); Supervision (equal); Writing – review & editing (equal).

DATA AVAILABILITY

The data that support the findings of this study are available within the article and its supplementary material.

REFERENCES

- S. J. Pearton, J. Yang, P. H. Cary, F. Ren, J. Kim, M. J. Tadjer, and M. A. Mastro, “A review of Ga_2O_3 materials, processing, and devices,” *Appl. Phys. Rev.* **5**(1), 011301 (2018).
- Z. Galazka, “ $\beta\text{-Ga}_2\text{O}_3$ for wide-bandgap electronics and optoelectronics,” *Semicond. Sci. Technol.* **33**(11), 113001 (2018).
- C. Wang, J. Zhang, S. Xu, C. Zhang, Q. Feng, Y. Zhang, J. Ning, S. Zhao, H. Zhou, and Y. Hao, “Progress in state-of-the-art technologies of Ga_2O_3 devices,” *J. Phys. D: Appl. Phys.* **54**(24), 243001 (2021).
- S. B. Reese and A. Zakutayev, *Proc. SPIE* **11281**, 112810H (2020).
- K. N. Heinselman, D. Haven, A. Zakutayev, and S. B. Reese, “Projected cost of gallium oxide wafers from edge-defined film-fed crystal growth,” *Cryst. Growth Des.* **22**(8), 4854–4863 (2022).
- E. M. Garrity, C.-W. Lee, P. Gorai, M. B. Tellekamp, A. Zakutayev, and V. Stevanović, “Computational identification of ternary wide-band-gap oxides for high-power electronics,” *PRX Energy* **1**(3), 033006 (2022).
- C. Venkata Prasad and Y. S. Rim, “Review on interface engineering of low leakage current and on-resistance for high-efficiency Ga_2O_3 -based power devices,” *Mater. Today Phys.* **27**, 100777 (2022).
- A. E. Islam, N. P. Sepelak, K. J. Liddy, R. Kahler, D. M. Dryden, J. Williams, H. Lee, K. Gann, A. Popp, K. D. Leedy, N. S. Hendricks, J. Brown, E. R. Heller, W. Wang, W. Zhu, M. O. Thompson, K. D. Chabak, and A. J. Green, “ 500°C operation of $\beta\text{-Ga}_2\text{O}_3$ field-effect transistors,” *Appl. Phys. Lett.* **121**(24), 243501 (2022).
- W. A. Callahan, E. Supple, D. Ginley, M. Sanders, B. P. Gorman, R. O’Hayre, and A. Zakutayev, “Ultrathin stable Ohmic contacts for high-temperature operation of $\beta\text{-Ga}_2\text{O}_3$ devices,” *J. Vac. Sci. Technol. A* **41**(4), 043211 (2023).
- K. Heinselman, P. Walker, A. Norman, P. Parilla, D. Ginley, and A. Zakutayev, “Performance and reliability of $\beta\text{-Ga}_2\text{O}_3$ Schottky barrier diodes at high temperature,” *J. Vac. Sci. Technol. A* **39**(4), 040402 (2021).
- T. Watahiki, Y. Yuda, A. Furukawa, M. Yamamuka, Y. Takiguchi, and S. Miyajima, “Heterojunction p- $\text{Cu}_2\text{O}/\text{n-Ga}_2\text{O}_3$ diode with high breakdown voltage,” *Appl. Phys. Lett.* **111**(22), 222104 (2017).
- Y. Zhang, Y. Li, Z. Wang, R. Guo, S. Xu, C. Liu, S. Zhao, J. Zhang, and Y. Hao, “Investigation of $\beta\text{-Ga}_2\text{O}_3$ films and $\beta\text{-Ga}_2\text{O}_3/\text{GaN}$ heterostructures grown by metal organic chemical vapor deposition,” *Sci. China Phys. Mech. Astron.* **63**(11), 117311 (2020).
- P. Sittimart, S. Ohmagari, T. Matsumae, H. Umezawa, and T. Yoshitake, “Diamond/ $\beta\text{-Ga}_2\text{O}_3$ pn heterojunction diodes fabricated by low-temperature direct-bonding,” *AIP Adv.* **11**(10), 105114 (2021).
- S. Nakagomi, K. Hiratsuka, Y. Kakuda, and K. Yoshihiro, “Beta-gallium oxide/SiC heterojunction diodes with high rectification ratios,” *ECS J. Solid State Sci. Technol.* **6**(2), Q3030–Q3035 (2017).
- T. Minami, Y. Nishi, and T. Miyata, “High-efficiency Cu_2O -based heterojunction solar cells fabricated using a Ga_2O_3 thin film as n-type layer,” *Appl. Phys. Express* **6**(4), 044101 (2013).
- M. Budde, D. Splith, P. Mazzolini, A. Tahraoui, J. Feldt, M. Ramsteiner, H. von Wenckstern, M. Grundmann, and O. Bierwagen, “ $\text{SnO}/\beta\text{-Ga}_2\text{O}_3$ vertical pn heterojunction diodes,” *Appl. Phys. Lett.* **117**(25), 252106 (2020).
- J. Zhang, S. Han, M. Cui, X. Xu, W. Li, H. Xu, C. Jin, M. Gu, L. Chen, and K. H. L. Zhang, “Fabrication and interfacial electronic structure of wide bandgap NiO and Ga_2O_3 p-n heterojunction,” *ACS Appl. Electron. Mater.* **2**(2), 456–463 (2020).
- X. Xia, J.-S. Li, C.-C. Chiang, T. J. Yoo, F. Ren, H. Kim, and S. J. Pearton, “Annealing temperature dependence of band alignment of NiO/ $\beta\text{-Ga}_2\text{O}_3$,” *J. Phys. D: Appl. Phys.* **55**(38), 385105 (2022).
- Y. Wang, H. Gong, Y. Lv, X. Fu, S. Dun, T. Han, H. Liu, X. Zhou, S. Liang, J. Ye, R. Zhang, A. Bu, S. Cai, and Z. Feng, “2.41 kV vertical p-NiO/n- Ga_2O_3 heterojunction diodes with a record Baliga’s figure-of-merit of $5.18 \text{ GW}/\text{cm}^2$,” *IEEE Trans. Power Electron.* **37**(4), 3743–3746 (2022).
- C. Wang, H. Gong, W. Lei, Y. Cai, Z. Hu, S. Xu, Z. Liu, Q. Feng, H. Zhou, J. Ye, J. Zhang, R. Zhang, and Y. Hao, “Demonstration of the p-NiO_x/n- Ga_2O_3 heterojunction gate FETs and diodes with $\text{BV}^2/\text{R}_{\text{on,sp}}$ figures of merit of $0.39 \text{ GW}/\text{cm}^2$ and $1.38 \text{ GW}/\text{cm}^2$,” *IEEE Electron Device Lett.* **42**(4), 485–488 (2021).
- H. Luo, X. Zhou, Z. Chen, Y. Pei, X. Lu, and G. Wang, “Fabrication and characterization of high-voltage NiO/ $\beta\text{-Ga}_2\text{O}_3$ heterojunction power diodes,” *IEEE Trans. Electron Devices* **68**(8), 3991–3996 (2021).
- X. Lu, X. Zhou, H. Jiang, K. W. Ng, Z. Chen, Y. Pei, K. M. Lau, and G. Wang, “1-kV sputtered p-NiO/n- Ga_2O_3 heterojunction diodes with an ultra-low leakage current below $1 \mu\text{A}/\text{cm}^2$,” *IEEE Electron Device Lett.* **41**(3), 449–452 (2020).
- X. Lu, Y. Deng, Y. Pei, Z. Chen, and G. Wang, “Recent advances in NiO/ Ga_2O_3 heterojunctions for power electronics,” *J. Semicond.* **44**(6), 061802 (2023).
- C. Liao, X. Lu, T. Xu, P. Fang, Y. Deng, H. Luo, Z. Wu, Z. Chen, J. Liang, Y. Pei, and G. Wang, “Optimization of NiO/ $\beta\text{-Ga}_2\text{O}_3$ heterojunction diodes for

- high-power application," *IEEE Trans. Electron Devices* **69**(10), 5722–5727 (2022).
- ²⁵Y. Kokubun, S. Kubo, and S. Nakagomi, "All-oxide p–n heterojunction diodes comprising p-type NiO and n-type β -Ga₂O₃," *Appl. Phys. Express* **9**(9), 091101 (2016).
- ²⁶H. Gong, X. Chen, Y. Xu, Y. Chen, F. Ren, B. Liu, S. Gu, R. Zhang, and J. Ye, "Band alignment and interface recombination in NiO/ β -Ga₂O₃ type-II p–n heterojunctions," *IEEE Trans. Electron Devices* **67**(8), 3341–3347 (2020).
- ²⁷Y. Deng, Z. Yang, T. Xu, H. Jiang, K. W. Ng, C. Liao, D. Su, Y. Pei, Z. Chen, G. Wang, and X. Lu, "Band alignment and electrical properties of NiO/ β -Ga₂O₃ heterojunctions with different β -Ga₂O₃ orientations," *Appl. Surf. Sci.* **622**, 156917 (2023).
- ²⁸A. Jain, S. P. Ong, G. Hautier, W. Chen, W. D. Richards, S. Dacek, S. Cholia, D. Gunter, D. Skinner, G. Ceder, and K. A. Persson, "Commentary: The Materials Project: A materials genome approach to accelerating materials innovation," *APL Mater.* **1**(1), 011002 (2013).
- ²⁹S. Ghosh, M. Baral, R. Kamparath, R. J. Choudhary, D. M. Phase, S. D. Singh, and T. Ganguli, "Epitaxial growth and interface band alignment studies of all oxide α -Cr₂O₃/ β -Ga₂O₃ p–n heterojunction," *Appl. Phys. Lett.* **115**(6), 061602 (2019).
- ³⁰S. Ghosh, M. Baral, J. Bhattacharjee, R. Kamparath, S. D. Singh, and T. Ganguli, "Evaluation of valence band offset and its non-commutativity at all oxide α -Cr₂O₃/ β -Ga₂O₃ heterojunction from photoelectron spectroscopy," *J. Appl. Phys.* **130**(17), 175303 (2021).
- ³¹S. Lany, "Band-structure calculations for the 3d transition metal oxides in *GW*," *Phys. Rev. B* **87**(8), 085112 (2013).
- ³²S. Lany, "Semiconducting transition metal oxides," *J. Phys.: Condens. Matter* **27**(28), 283203 (2015).
- ³³V. Stevanović, S. Lany, X. Zhang, and A. Zunger, "Correcting density functional theory for accurate predictions of compound enthalpies of formation: Fitted elemental-phase reference energies," *Phys. Rev. B* **85**(11), 115104 (2012).
- ³⁴C. J. Bartel, S. L. Millican, A. M. Deml, J. R. Rumptz, W. Tumas, A. W. Weimer, S. Lany, V. Stevanović, C. B. Musgrave, and A. M. Holder, "Physical descriptor for the Gibbs energy of inorganic crystalline solids and temperature-dependent materials chemistry," *Nat. Commun.* **9**(1), 4168 (2018).
- ³⁵C. W. Bale, E. Bélisle, P. Chartrand, S. A. Deckerov, G. Eriksson, A. E. Gheribi, K. Hack, I.-H. Jung, Y.-B. Kang, J. Melançon, A. D. Pelton, S. Petersen, C. Robelin, J. Sangster, P. Spencer, and M.-A. Van Ende, "FactSage thermochemical software and databases, 2010–2016," *Calphad* **54**, 35–53 (2016).
- ³⁶J. Osorio-Guillén, S. Lany, S. V. Barabash, and A. Zunger, "Magnetism without magnetic ions: Percolation, exchange, and formation energies of magnetism-promoting intrinsic defects in CaO," *Phys. Rev. Lett.* **96**(10), 107203 (2006).
- ³⁷C.-W. Lee, A. Zakutayev, and V. Stevanović, "Computational insights into phase equilibria between wide-gap semiconductors and contact materials," *arXiv:2312.11749* (2023).
- ³⁸E. Arca, K. Fleischer, S. A. Krasnikov, and I. Shvets, "Effect of chemical precursors on the optical and electrical properties of p-type transparent conducting Cr₂O₃:(Mg,N)," *J. Phys. Chem. C* **117**(42), 21901–21907 (2013).
- ³⁹K. Fleischer, D. Caffrey, L. Farrell, E. Norton, D. Mullarkey, E. Arca, and I. V. Shvets, "Raman spectra of p-type transparent semiconducting Cr₂O₃:Mg," *Thin Solid Films* **594**, 245–249 (2015).
- ⁴⁰E. Arca, A. B. Kehoe, T. D. Veal, A. Shmeliov, D. O. Scanlon, C. Downing, D. Daly, D. Mullarkey, I. V. Shvets, V. Nicolosi, and G. W. Watson, "Valence band modification of Cr₂O₃ by Ni-doping: Creating a high figure of merit p-type TCO," *J. Mater. Chem. C* **5**(47), 12610–12618 (2017).
- ⁴¹K. A. Borup, E. S. Toberer, L. D. Zoltan, G. Nakatsukasa, M. Errico, J.-P. Fleurial, B. B. Iversen, and G. J. Snyder, "Measurement of the electrical resistivity and Hall coefficient at high temperatures," *Rev. Sci. Instrum.* **83**(12), 123902 (2012).
- ⁴²W. Hao, Q. He, X. Zhou, X. Zhao, G. Xu, and S. Long, in *IEEE 34th International Symposium on Power Semiconductor Devices and ICs (ISPSD) Vancouver, BC (IEEE, 2022)*, pp. 105–108.
- ⁴³L. Zhou, X. Lu, L. Chen, X. Ouyang, B. Liu, J. Xu, and H. Tang, "Leakage current by Poole–Frenkel emission in Pt Schottky contacts on (201) β -Ga₂O₃ grown by edge-defined film-fed growth," *ECS J. Solid State Sci. Technol.* **8**(7), Q3054–Q3057 (2019).
- ⁴⁴S. M. Sze, Y. Li, and K. K. Ng, *Physics of Semiconductor Devices* (John Wiley & Sons, 2021).
- ⁴⁵Z. Wang, H.-H. Gong, X.-X. Yu, X. Ji, F.-F. Ren, Y. Yang, S. Gu, Y. Zheng, R. Zhang, and J. Ye, "Trap-mediated bipolar charge transport in NiO/Ga₂O₃ p⁺–n heterojunction power diodes," *Sci. China Mater.* **66**(3), 1157–1164 (2023).
- ⁴⁶A. M. E. Raj, M. Jayachandran, and C. Sanjeeviraja, "Fabrication techniques and material properties of dielectric MgO thin films—A status review," *CIRP J. Manuf. Sci. Technol.* **2**(2), 92–113 (2010).
- ⁴⁷Z. Liu, J. Yu, P. Li, X. Wang, Y. Zhi, X. Chu, X. Wang, H. Li, Z. Wu, and W. Tang, "Band alignments of β -Ga₂O₃ with MgO, Al₂O₃ and MgAl₂O₄ measured by x-ray photoelectron spectroscopy," *J. Phys. D: Appl. Phys.* **52**(29), 295104 (2019).